Title

Imaging Active Urokinase Plasminogen Activator in Prostate Cancer

Journal

Cancer Research, 75(7)

ISSN

0008-5472

Authors

LeBeau, Aaron M

Sevillano, Natalia

Markham, Kate

et al.

Publication Date

2015-04-01

DOI

10.1158/0008-5472.can-14-2185

Peer reviewed

Published in final edited form as:

Cancer Res. 2015 April 1; 75(7): 1225–1235. doi:10.1158/0008-5472.CAN-14-2185.

Imaging Active Urokinase Plasminogen Activator in Prostate Cancer

Aaron M. LeBeau[1,*,4], **Natalia Sevillano**[2,4], **Kate Markham**[3], **Michael B. Winter**[2], **Stephanie T. Murphy**[1], **Daniel R. Hostetter**[3], **James West**[3], **Henry Lowman**[3], **Charles S. Craik**[2], and **Henry F. VanBrocklin**[1]

[1]Center for Molecular and Functional Imaging, Department of Radiology and Biomedical Imaging, University of California, San Francisco, San Francisco, California USA

[2]Department of Pharmaceutical Chemistry, University of California, San Francisco, San Francisco, California USA

[3]CytomX Therapeutics Inc., South San Francisco, California USA

Abstract

The increased proteolytic activity of membrane-bound and secreted proteases on the surface of cancer cells and in the transformed stroma is a common characteristic of aggressive metastatic prostate cancer. We describe here the development of an active site-specific probe for detecting a secreted peritumoral protease expressed by cancer cells and the surrounding tumor microenvironment. Using a human fragment antigen binding phage display library, we identified a human antibody termed U33 that selectively inhibited the active form of the protease urokinase plasminogen activator (uPA, *PLAU*). In the full-length immunoglobulin form, U33 IgG labeled with near-infrared fluorophores or radionuclides allowed us to non-invasively detect active uPA in prostate cancer xenograft models using optical and single-photon emission computed tomography (SPECT) imaging modalities. U33 IgG labeled with ^{111}In had a remarkable tumor uptake of 43.2% injected dose per gram (%ID/g) 72hr post tail vein injection of the radiolabeled probe in subcutaneous xenografts. Additionally, U33 was able to image active uPA in small soft-tissue and osseous metastatic lesions using a cardiac dissemination prostate cancer model that recapitulated metastatic human cancer. The favorable imaging properties were the direct result of U33 IgG internalization through an uPA receptor mediated mechanism where U33 mimicked the function of the endogenous inhibitor of uPA to gain entry into the cancer cell. Overall, our imaging probe targets a prostate cancer-associated protease, through a unique mechanism, allowing for the non-invasive preclinical imaging of prostate cancer lesions.

Address Correspondence to: Aaron M. LeBeau, Ph.D., Department of Pharmacology, University of Minnesota Masonic Cancer Center, 6-120 Jackson Hall, 321 Church St. SE, Minneapolis, MN, 55455-0217, Phone: (612) 301-7231, Fax: (612) 625-8408, alebeau@umn.edu. Henry F. VanBrocklin, Ph.D., Department of Radiology and Biomedical Imaging, University of California, San Francisco, 185 Berry Street, Suite 350, San Francisco, CA, 94143-2280, Phone: (415) 353-4569, Fax: (415) 514-8242, Henry.Vanbrocklin@ucsf.edu.

*Current address: Department of Pharmacology, University of Minnesota Masonic Cancer Center, Minneapolis, Minnesota USA.

[4]These authors contributed equally to this work.

The authors declare no conflict of interest

Keywords

urokinase plasminogen activator; prostate cancer; imaging of tumor progression and metastasis; protease-inhibitor systems; non-invasive imaging of animal models

Introduction

Prostate cancer afflicts men in the western world at rates greater than any other malignancy resulting in the deaths of ~30,000 men annually (1). Androgen ablation therapy is an effective treatment for men with hormone-sensitive prostate cancer. Despite high initial response rates, a majority of men undergoing androgen ablation relapse leading to castration-resistant prostate cancer (CRPC) (2). Recent drug approvals by the FDA have demonstrated the impact that novel therapies can have on improving the quality and quantity of life for men with CRPC (3). Men with metastatic CRPC, however, are still likely to die from this disease and therefore, better therapies are needed. The development of novel therapies and the efficient use of established therapies are hindered by poor measures of response. Sensitive non-invasive imaging probes that identify cancerous lesions and measure cancer cell viability post-therapy would allow physicians to rapidly assess treatment efficacy and provide personalized care for men suffering from CRPC.

The ability to accurately image metastatic prostate cancer in soft tissue and bone remains an unmet clinical need. Modalities such as CT and MRI require large anatomical changes to be effective and provide limited information regarding the underlying tumor physiology (4). Dynamic hyperpolarized carbon-13 MRI has been used to characterize tumor metabolism in patients with organ-confined prostate cancer, but it is not yet available for imaging metastases (5). Radionuclide bone scans, which measure bone remodeling, are common for evaluating metastatic cancer and therapeutic response. However, false-positives are common with bone scans since remodeling can occur from pre-existing bone trauma, inflammation and arthritis (6). The FDA approved metabolic imaging tracer, ^{18}F-fluorodexoyglucose, has met with limited success imaging prostate cancer because of the changing metabolic signatures at different stages of the disease (7). Other metabolic agents including ^{11}C-choline, ^{18}F-fluorocholine, ^{11}C-acetate, ^{11}C-methionine, ^{18}F-1-(2-Deoxy-2-fluoro-β-L-arabinofuranosyl)-5-methyluracil) (FMAU), 1-amino-3-^{18}F-fluorocyclobutane-1-carboxylic acid (^{18}F-FACBC), and ^{18}F-Fluorothymidine for measuring membrane synthesis, fatty acid transport, amino acid transport/protein synthesis, and proliferation, respectively, continue to be investigated (8, 9). The lack of an identifiable metabolic phenotype has led to the selective targeting of proteins over-expressed by prostate cancer. One such example is the FDA approved ProstaScint, a murine antibody for SPECT imaging that binds the metalloprotease prostate-specific membrane antigen (PSMA) (10). ProstaScint recognizes an intracellular epitope of PSMA allowing the antibody to only image cells that are dead or undergoing necrosis. The resulting scans are of poor quality and limited to lymph node staging (11). Next generation antibodies and small-molecules labeled with PET and SPECT isotopes targeting the extracellular PSMA domain have shown promise in early human trials (12, 13).

The plasminogen activation system (PAS) is an attractive target for a biomarker-based imaging strategy for CRPC. Over-expression of the PAS – which consists of the serine protease urokinase plasminogen activator (uPA), the uPA receptor, uPAR, and uPA inhibitor, PAI-1, – has been documented in primary and metastatic prostate cancer (14–16). Central to the role of the PAS in prostate cancer is the proteolytic activity of uPA. Importantly, uPA activity has been implicated in the formation of osteoblastic bone lesions and in prostate cancer with increased metastatic potential (14, 16, 17). Enzymatically active uPA has been isolated and characterized in CRPC bone metastases and in primary prostate cancer tumors (18). Upon secretion by cancer cells, uPA exists as inactive pro-uPA that is converted to its active form by proteases in the pericellular milieu. uPA binding to uPAR results in the accelerated conversion of plasminogen to plasmin. Plasmin can then directly cleave basement membrane proteins, or activate other proteases, leading to dissolution of the extracellular membrane. Inhibition of active uPA by PAI-1 results in the internalization of the uPA/uPAR/PAI-1 complex. Studies have shown that PAI-1, independent of uPA, functions as a signaling molecule by interacting with cell surface receptors (19). PAI-1 can also be inactivated by other prostate cancer-associated proteases, such as human kallikrein 2 (20). These studies suggest that little functional PAI-1 exists to inactive the PAS resulting in high levels of active uPA in prostate cancer.

Several groups have investigated uPA as a prostate cancer biomarker in the serum and by immunohistochemical analysis of diseased tissue. Circulating levels of uPA in the serum of prostate cancer patients have been found to directly correlate with cancer stage and metastasis (21, 22). From studies using prostate cancer tissue microarrays, uPA was found to be ubiquitously expressed in organ-confined and metastatic cancer (23, 24). Additionally, overexpression of uPA and its inhibitor PAI-1 were found to be associated with aggressive cancer recurrence post-prostatectomy by IHC (25, 26). Encouraged by these data we hypothesize that enzymatically active uPA can be selectively targeted for preclinical imaging in prostate cancer models. In this report, the development of a new technology for imaging prostate cancer centered on active uPA is detailed. Using a human fragment antigen-binding (Fab) phage display library, the active-site binding inhibitory antibody (termed U33) was discovered. U33 IgG was found to be a potent and selective inhibitor of uPA, displaying no affinity towards homologous proteases. Through a novel mechanism, we show that U33 IgG results in the internalization of uPA by uPAR, thereby mimicking the action of its endogenous inhibitor PAI-1. Labeled with a near-infrared (NIR) dye for optical imaging or ^{111}In for SPECT, U33 IgG was used to detect active uPA *in vivo* in prostate cancer xenografts and in experimental mestatasis models. Due to its internalization, U33 IgG demonstrated high tumor retention *in vivo* with high signal to noise. These preclinical data presented justify a clinical trial to assess the impact of U33 IgG at imaging CRPC in men.

Materials and Methods

Cell Culture

All cancer cells lines used in this study were purchased from American Type Culture Collection (ATCC) and were maintained in their respective recommended media,

supplemented with 10% FBS, 100 U/ml penicillin, and 100 μg/ml streptomycin at 37°C. The cell lines were authenticated using short-tandem repeat profiling provided by the vendor. The uPAR knockout cell line was generated using uPAR shRNA Plasmid (h): sc-36781-SH from Santa Cruz. Transfection was performed with a lentiviral particle according to the manufacturer's protocol. Following puromycin treatment, clones were selected using flow cytometry with an AlexaFluor 488 labeled anti-uPAR antibody (27). Gene expression of the clone used for the xenograft study was analyzed using qPCR and flow cytometry.

Quantitative PCR

RNA was prepared from each cell line (~ 2×10^6 cells/cell line) using an RNEasy kit (Qiagen). Following RNA isolation, each sample was treated with Turbo DNA-free (Ambion) to remove any residual DNA. RNA was synthesized to cDNA using the High Capacity RNA-to-cDNA kit (Applied Biosystems). For each gene, the Taqman qPCR was performed in quadruplicate using the Taqman Universal PCR Master Mix (Applied Biosystems). The following Taqman Gene Expression Assay probes were used: uPAR – Hs00182181_m1 PLAUR, uPA – Hs01547054_m1 PLAU, PAI-1 Hs01126606_m1 and 18s ribosomal 1 (reference gene) Hs03928985_g1 RN18S1. All qPCR was performed on an ABI 7300 Real Time PCR system instrument. Data were analyzed using the comparative Ct method (fold change = $2^{-\Delta\Delta Ct}$) (28).

Histology

Immnofluoresence was performed on prostate cancer tissue microarrays purchased from US Biomax, Inc (PR959). uPA was detected with antibody sc-14019 (Santa Cruz) (1:100) following the manufacturer's recommendation using an anti-rabbit AlexaFluor 488 conjugated secondary. The protocol for antigen retrieval and staining for e-cadherin was previously published (29).

Phage Display Panning

A fully human naïve Fab phage display library was used to identify inhibitory antibodies against human active uPA (30). Recombinant Human uPA (R&D Systems) was immobilized overnight in wells of a MaxiSorp® flat-bottom 96 well plate (Nunc) at 20 μg/mL in PBS (137 mM NaCl, 2.7 mM KCl, Na_2HPO_4, 10 mM, KH_2PO_4 2 mM pH 7.4). The panning was accomplished in four rounds as described previously (31, 32). After four rounds of selection, Fab was produced from 192 individual clones in a 96-well format, the Fabs that leaked into the cell culture media were screened for binding to uPA by ELISA. Clones with a positive signal in ELISA were analyzed by *Bst*NI restriction analysis to identify the unique clones. Clones with unique sequence were expressed, purified, and tested for inhibition of uPA.

IgG Production

The heavy chain and light chain variable domains of U33 Fab sequence were cloned separately into pcDNA3.1 derived human IgG1 expression vectors, co-transfected into 293 F cells (Life Technologies) cells, and selected with both hygromycin and neomycin for 14 days. The stable cells were then subcloned and a high U33 antibody-expressing cell line,

8G4, was obtained. This cell line was expanded and grown in FreeStyle 293 medium (Life Technologies) using Wave System (GE) and supernatants were harvested after 10–12 days' culture. IgG was purified using a MabSelect SuRe Protein A column (GE), and followed by preparative size exclusion chromatography using a HiPrep 16/60 Sephacryl S-200 HR column (GE).

ELISA

MaxiSorp® plates were coated with 50 μL of 5 μg/mL recombinant Human uPA (in some experiments the zymogen, single chain uPA- pro-urokinase, or mouse uPA was used) in PBS overnight at 4°C. The unbound uPA was removed and the plate was washed with PBS and blocked with milk-PBS. Supernatants of Fab induced cultures or serial dilutions of pure Fab ranging from 1 μM to 0, were added to each well and incubated for 1 hour. Wells were washed with PBS-Tween and the Fab was detected with anti-myc antibody conjugated to peroxidase (Roche) and TMB reagent (Pierce). The absorbance was determined at 450 nm using a microplate reader.

Kinetic Assays

Human uPA (6.2 nM) was incubated with 1 μM of Fab in assay buffer (50 mM Tris pH 8.8, 0.01% Tween 20), after 1 hour of incubation at room temperature, the chromogenic substrate Spectrozyme®uPA (American Diagnostica, Inc) at a final concentration of 50 μM was added. The reaction velocity was monitored by reading the absorbance at 405 nm. For the Ki calculation, 6.2 nM of uPA was incubated with Fab (0–2μM) in assay buffer at room temperature for 5hrs. uPA activity was measured for each inhibitor concentration by addition of substrate (3.9 μM–500 μM). All data were analyzed using Graphpad Prism software. Inhibition of uPA bound to uPAR: uPAR was immobilized in wells of a MaxiSorp® plate. 2.5μg/mL of uPA was added to uPAR-coated plates and incubated for 1 hour. After washing, serial dilutions of pure Fab ranging from 1 μM to 16 nM were added to the wells and incubated for 1hour. For the specificity assays U33 IgG was used at concentrations ranging from 2 μM to 0.010 μM. Protease concentrations and fluorogenic substrates were used as previously described for the specificity assay (33).

Internalization

Cancer cell lines (30,000 cells per well in 12-well plates in triplicate) were incubated in conditioned media (protein concentration of 5μg/ml) with 10 nM (0.1μCi) ^{111}In-U33 or ^{111}In-A11 for 0 to 4 hr at 4°C and 37°C. At the indicated time, the media was removed and the cells were washed with a mild acid buffer [50 mM glycine, 150 mM NaCl (pH 3.0)] at 4°C for 5 min. Cells were tryspinized and pelleted at 20,000g for 5 min. The supernatant (containing cell surface bound radioactivity) and the cell pellet (containing internalized radioactivity) were counted on a Gamma counter.

Mass Spectrometry

Protein identification of conditioned media was carried out as described with the following notable exceptions (34). Conditioned media samples (4 ug) were digested with trypsin (1:20 trypsin to protein ratio). Extracted peptides were sequenced with an LTQ-FT ICR mass

spectrometer (Thermo Scientific). SwissProt database searches were conducted with mass tolerances of 20 p.p.m for parent ions and 0.6 Da for fragment ions using maximum expectation values of 0.01 for protein and 0.05 for peptide matches.

Animal Models

The animal work was in accordance with a UCSF Institutional Animal Care and Use Committee protocol. Six to seven-week-old nu/nu mice were purchased from Taconic Farms. Nude mouse xenografts were generated by subcutaneous injection of each cell line (1×10^6 cells/ml; 100 μl per site/mouse). Animals for imaging and biodistribution studies had tumor volumes between 100 – 350 mm^3. The intracardiac dissemination model was generated using the previously described method (35).

In vivo optical imaging

U33 IgG was labeled with AlexFluor 680 and characterized *in vivo* using a previously published method. Images were collected in fluorescence mode on an IVIS 50 (Caliper/Xenogen) using Living Image 2.50.2 software at 24 hour intervals. Region of interest measurements were made and the fluorescence emission images were normalized to reference images and the unitless efficiency was computed. For bioluminescence imaging, the mice were injected with intraperitoneally with D-luciferin (150 mg/kg body weight). Images were acquired 10 min after the injection of D-luciferin and the total flux (p s-1) in the region of interest was measured. For one PC3 xenograft, the tumor was removed at 72hr and frozen in OCT. Blocks were cut into 8μm sections, fixed in acetone for 10 minutes at −20°C and mounted using ProLong Gold with DAPI. Probe localization was visualized in the Cy7 channel using a Nikon 6D High Throughput Epifluorescence Microscope.

Radiolabelling and SPECT/CT Imaging

SPECT/CT—The chelate group for ^{111}In, 1,4,7,10-Tetraazacyclododecane-1,4,7,10-tetraacetic acid N-hydroxysuccinimide ester (DOTA-NHS) (Macrocyclics), was attached to lysine residues on the IgG using a 25:1 molar excess of chelate in a 0.1 M NaHCO3, pH 9.0 buffer with an antibody concentration of 6 mg/ml. After two hours of labeling at room temperature, the antibody-DOTA conjugate was FPLC purified to remove unreacted DOTA-NHS. For ^{111}In radiolabeling, $^{111}InCl_3$ was purchased from Perkin Elmer (Shelton, CT). To radiolabel the IgG, 50 μg of DOTA conjugate in 0.2 M ammonium acetate (pH 6.0) was incubated with 12μl of $InCl_3$ (2.10 mCi) in 0.1 N HCl for 60 minutes at 40°C. The labeled products were purified using a PD-10 column pre-equilibrated with PBS buffer. Labeling efficiency and purity of the product were determined using thin-layer chromatography. The specific activity of ^{111}In-U33 IgG was calculated to be 31.6 ± 4 mCi/mg (n = 4). For imaging, 2.5 – 5.0 μg of probe, corresponding to 275–360 μCi of activity, were injected into the tail vein. The mice were imaged using a Gamma Medica Ideas XSPECT SPECT/C system. Reconstructed data were analyzed with AMIDE and AMIRA software.

Biodistribution study

Mice (n = 4/time point) bearing PC3 and CWR22Rv1 xenografts were injected with 25 μCi (2.5 μg) of ^{111}In-U33 IgG. At 24, 48 and 72hrs, the animals were euthanized for analysis in

accordance with UCSF Animal Care and Use Committee guidelines. Blood was collected by cardiac puncture. The tumor, heart, lung, spleen, kidneys, and muscle were harvested, weighed and counted in an automated γ-counter (Wizard2; Perkin Elmer). The percentage injected dose per gram (% ID/g) of tissue was calculated by comparison with standards of known radioactivity.

Results

Identification of urokinase plasminogen activator in prostate cancer

Quantitative PCR (qPCR) determined that PAS expression was highest in the androgen independent metastatic prostate cancer cell lines, PC3 and DU145 (Fig. 1A). Little or no expression was documented in other prostate cancer cells lines, normal prostate epithelial cells (PrEC) and in the bladder cancer cell line TSU. Out of the two cell lines that expressed the PAS, the mRNA expression of uPAR and uPA were highest in PC3 cells, while DU145 cells expressed significantly higher PAI-1. Data have demonstrated that over-expression of the PAS can induced by hypoxia in breast cancer models and that hypoxia is common in prostate cancer (36, 37). PC3 and DU145 cells were cultured in 1.5% O_2, to mimic the O_2 deprived environment of prostate cancers, and the levels of the PAS were analyzed (Fig. 1B) (38, 39). After 72hrs, hypoxia had induced a two-fold increase in expression of the PAS members in PC3 cells. DU145 cells were less affected by hypoxia with only uPAR expression increased.

The presence of uPA at the protein level was next investigated in tissue sections taken from subcutaneous PC3 and DU145 xenografts using IHC. A commercially available antibody (sc-14019) that recognized total uPA protein (zymogen uPA, active uPA and PAI-1 bound uPA) detected uPA in both xenograft sections with more intense staining visible in the PC3 section (Fig. 1C). Total uPA protein was next visualized in a prostate cancer tissue microarray using immunofluorescence (IF) (Fig. 1D – G). Total uPA protein was detected in adenocarcinomas and in osseous metastases with IF using the antibody sc-14019. Of the tumor sections found to be positive for uPA, 70% (28/40) were found to Gleason score 7 or higher. This finding mirrored an earlier report by Cozzi, et al. that found that 76% of the uPA positive tumors were Gleason score & or higher (24). In concordance with previous work, we documented that uPA was located in both the epithelium and stroma (14, 40).

U33 antibody development

A human naïve B cell phage display library with a diversity of 4.1×10^{10} was used to identify inhibitory antibodies against human uPA. After four rounds of panning, 192 independent clones were screened by ELISA. Of these clones, 67 showed high ELISA signals and 23 had unique sequences. The 23 unique clones identified were expressed, purified, and tested for uPA inhibition. Clone U33 was the only Fab that exhibited inhibitory activity with sequence of U33 Fab shown in Supplemental Fig. 1. The affinity and specificity of U33 Fab were determined by quantitative ELISA and fluorogenic inhibition assays using human uPA (active and zymogen) and mouse uPA. ELISA results showed that U33 Fab bound to active uPA in a concentration-dependent manner, but not zymogen uPA or mouse uPA (Fig. 2A). The inhibition data using a fluorogenic substrate in Fig. 2B showed

that U33 Fab inhibits more than 80% of human uPA activity and has no effect on the mouse enzyme.

Under steady-state conditions U33 Fab possessed a K_i of 20nM for soluble uPA (Supplemental Fig. 2) and was also able to inhibit uPA bound to uPAR (Fig. 2C). Further characterization studies were performed and found that U33 Fab could block binding of uPA to its endogenous inhibitor PAI-1 in a dose dependent manner (Fig. 2D), but was unable to dislodge PAI-1 in a preformed uPA/PAI-1 complex (Supplemental Fig. 3). The mechanism of inhibition of uPA by U33 Fab was next investigated. Active uPA was pretreated with the irreversible active site inhibitor Glu-Gly-Arg-chloromethyl ketone (CMK). When added to the uPA-CMK complex, the binding of U33 Fab to uPA was significantly decreased suggesting that U33 Fab required a free unoccupied active site for binding and inhibition (Fig. 2E). The heavy and light chain variable domains of U33 Fab were cloned into a full-length IgG1 expression vector, co-transfected into 293 F cells, expressed and purified. Kinetic analysis using double reciprocal plots revealed that U33 IgG was a competitive inhibitor of uPA with a K_i of 10nM (Fig. 2F). Additional characterization studies of U33 IgG were performed (Supplemental Fig. 4) and it was found that U33 IgG could displace the non-covalent small molecule inhibitor p-aminobenzamidine in the active site of uPA when incubated with inhibited protease (Supplemental Figure 5).

U33 IgG *in vitro* characterization

U33 IgG was specific for uPA when assayed against a panel of proteases using a fluorogenic substrate inhibition assay. No cross reactivity was observed with proteases displaying an array of specificities, including the prostate cancer-associated serine proteases hK2, PSA and KLK4 (Fig. 3A and Supplemental Fig. 6). U33 IgG was tested for its ability to inhibit trypsin-like proteolysis in PC3 and DU145 conditioned media (Fig. 3B). When incubated with the generic trypsin fluorogenic substrate, Z-Gly-Gly-Arg-AMC, PC3 and DU145 conditioned media showed substantial trypsin-like activity. Addition of 100nM U33 IgG inhibited all trypsin-like proteolytic activity. Proteomic analysis of the secreted proteases in the conditioned media found that both cells lines had high levels of uPA (Fig. 3C). The other proteases identified in the conditioned media did not display activity against the substrate, were not active at physiological pH, or might have been in an inactive state such as zymogen.

U33 IgG labeled with ^{111}In via a DOTA chelate (^{111}In-U33 IgG) was internalized by PC3 cells at 37°C with 72% of the total radioactivity internalized within 120 minutes (Fig. 3D). A study conducted at the 120 minute time point found that ^{111}In-U33 IgG internalization was dependent on the presence of active uPA and uPAR (Fig. 3E). Internalization was observed in DU145 cells- but was blocked in PC3 and DU145 cells pretreated with excess cold U33 IgG. Internalization was not observed in PC3 cells with uPAR expression knocked out. In PC3 cells expressing both active uPA and uPAR, ^{111}In-U33 IgG internalization was prevented by the addition of an antagonistic uPAR antibody (2G10) that blocks uPA binding to uPAR. No internalization occurred in CWR22Rv1cells and in PC3 cells treated with the isotype control ^{111}In-A11 IgG.

U33 IgG *in vivo* imaging

Encouraged by the *in vitro* data, U33 IgG was tested for its ability to detect active uPA *in vivo* using NIR optical imaging. U33 IgG labeled with AlexaFluor 680 (AF680-U33 IgG) allowed for the qualitative detection of active uPA in xenografts (Fig. 4A). Maximum probe localization was achieved at 72hrs with the PC3 xenograft demonstrating high tumor uptake and retention. Lower tumor uptake was observed in the DU145 xenograft corroborating the mRNA and IHC results. No probe localization was present in the CWR22Rv1 xenograft. Cryosectioning of the PC3 tumor at 72hrs, and subsequent imaging of AF680-U33 IgG with fluorescence microscopy, found probe penetration in the tumor tissue (Fig. 4B). The accumulation of the probe in the tumor was greater than in the liver, the main clearance organ for IgG antibodies (Fig. 4C). Graphing the fluorescence efficiency of the regions of interest for each of the mice imaged as a function of time highlighted the uptake kinetics and selectivity of the probe (Fig. 4D).

The clinically relevant imaging modality SPECT/CT was next used to acquire three dimensional tomographic data. ^{111}In-U33 IgG localization was seen 72hrs post-injection in the PC3 xenograft as documented by a pronounced tumor signal in the 3D data reconstruction and the 2D transverse view of the fused SPECT/CT image (Fig. 4E). In the SPECT/CT images, noticeable hepatic clearance of the probe was observed with little secondary accumulation in other locations. A biodistribution study of ^{111}In-U33 IgG in the PC3 xenograft found that the probe accumulated preferentially over time in the tumor with a %ID/g of 43.2% at 72hrs (Fig. 4F). ^{111}In-U33 IgG had low background *in vivo* with a tumor-to-blood ratio of 9.9 and a tumor-to-muscle ratio of 63. When treated with excess cold U33 IgG (200μg) prior to radiotracer injection, probe accumulation was blocked 80% at 72hrs post-injection (Fig. 4G.). No uptake of ^{111}In-U33 IgG was found in the CWR22Rv1 xenograft with a %ID/g of 4.8% representing non-specific tumor localization at 72hrs.

^{111}In-U33 IgG was tested for its ability to detect small lesions that mimic human prostate cancer using a PC3 intracardiac dissemination model. The PC3 cells used for this model were engineered to stably express luciferase and the formation of experimental metastatic lesions was monitored by bioluminescence imaging (BLI) after injection of luciferin. By week six, distinct experimental metastases had formed in the bone, brain and lymph nodes of the mice. ^{111}In-U33 IgG imaged a pronounced osseous lesion in the jaw of this model that was identified by BLI (Fig. 5A). In the 2D and 3D reconstructed views, the lesion (11.6 mm^3 volume) was located in the left mandible. The lesion was homogenized and the supernatant had marked trypsin-like proteolytic activity, when incubated with the fluorogenic trypsin substrate, compared to normal control tissue extracted from the right mandible (Fig. 5B). This proteolytic activity was inhibited by the addition of 100nM U33 IgG. In another example, ^{111}In-U33 IgG was able to resolve a lesion from the skull infiltrating the brain (28.3 mm^3 volume) identified by BLI (Fig. 5A). Staining of the lession for Ki-67 found that the lesion was highly proliferative compared to adjacent normal tissue (Fig. 5C). In addition to the skull-brain lesion, the 2D and 3D reconstructed views also showed the detection of lymph node lesions that were obscured by the intense signal coming from the brain lesion in the BLI image (Fig. 5A).

Discussion

In this article, the development of the SPECT imaging probe, U33 IgG, is documented from its initial discovery, using a human antibody identified from a Fab phage display library, to its preclinical evaluation *in vivo* in prostate cancer models. Targeting the active form of uPA, U33 IgG detects a serine protease found extensively in prostate cancer. In healthy prostate tissue, the uPA promoter is epigenetically silenced by hypermethylation resulting in no detectable uPA in the prostate (41, 42). As prostate cancer progresses, methylation patterns change and uPA is expressed (42). High levels of uPA protein in tumor tissue and serum have directly correlated with cancer progression, metastasis and poor clinical outcome in men with prostate cancer (23–25, 43, 44). *In vitro* uPA expression was highest in the androgen independent cell lines PC3 and DU145 and expression was significantly increased in PC3 cells under hypoxia. Prostate cancer cell lines that express androgen receptor (AR) can be induced to express uPA when treated with demethylating agents. LNCaP cells challenged with 5-azacytidine were found to turn on uPA expression resulting in cells that were more proliferative and invasive than the parental line *in vitro* and *in vivo* (42). Although only expressed in two clonal derived cell lines, immunofluorescence found total uPA protein was present in prostate tumors of every grade and in both soft tissue and osseous metastases. These data support and further validate the earlier findings attesting to the presence of uPA in both AR positive and AR negative prostate cancer and also speak to the paucity of good *in vitro* models that accurately reflect human disease in prostate cancer research (23–25, 40, 45).

The development of uPA inhibitors has mainly focused on low molecular weight compound (46–48). The further translation of these molecules has been prevented by poor specificity and off-target effects. A previous attempt to develop an inhibitory antibody for uPA gave a human monoclonal antibody with a low nanomolar affinity (49). This antibody could not, however, distinguish between active uPA and pro-uPA and lacked species specificity. Studies with U33 Fab found the antibody could inhibit both secreted and uPAR bound uPA in the low nanomolar range and was specific for the active human form. U33 Fab could not bind to uPA inhibited by PAI-1 or displace PAI-1 from the complex. Inhibition studies against other proteases, including S1A proteases associated with prostate cancer, found U33 IgG to be a specific, competitive inhibitor of uPA. Further evidence for U33 binding to the active site was provided by use of active site-directed uPA inhibitors. U33 IgG could displace a non-covalent small-molecule inhibitor from the S1 pocket of uPA and pre-incubation of uPA with a covalent CMK inhibitor blocked U33 binding. Based on these data, we demonstrate that U33 specifically targets active uPA *in vitro* and *in vivo* with an accuracy not seen with other uPA inhibitory antibodies or small-molecules.

The imaging properties of U33 IgG *in vivo* were characteristic of antibody imaging probes that target membrane proteins. Although targeting a secreted protein, U33 IgG demonstrated high tumor uptake and retention in uPA/uPAR-expressing xenografts by NIR and SPECT imaging. U33 IgG was sensitive enough to detect small osseous and soft tissue metastatic lesions a few millimeters in size using SPECT/CT. Key to the success of U33 IgG as an imaging probe was its internalization through an uPAR mediated mechanism. Internalization was blocked with excess cold U33 IgG and not observed in PC3 cells with uPAR expression

knocked out or in PC3 cells with the uPA-uPAR binding epitope blocked by an antibody. These results suggest an internalization mechanism requiring active uPA and uPAR, with U33 IgG mimicking PAI-1. Both PAI-1 and U33 IgG bind to the C-terminal protease domain while uPAR binds to the N-terminal domain of uPA. Furthermore, PAI-1 inhibition of uPA bound uPAR results in internalization of the uPA/uPAR/PAI-1 complex. *In vivo* the internalization mechanism of U33 IgG afforded probe accumulation and sequestration in tumor tissue. Internalization prevented the dissemination of uPA-U33 IgG complex to peripheral tissue resulting in high tumor uptake values that increased over time as demonstrated by the biodistribution. The internalization of U33 IgG is in direct contrast to a recent study that targeted another secreted protease, PSA, for PET imaging using a murine IgG antibody (^{89}Zr-5A10) (50). With no means of internalization or bioaccumulation, ^{89}Zr-5A10 uptake reached its maximum uptake 24hrs post-injection with a low tumor-to-blood ratio. There are no published reports of an antibody that binds to a protease receptor ligand mimicking the activity of the endogenous inhibitor and causing the internalization of the antibody/ligand/receptor complex.

Several research groups have imaged the PAS by targeting the uPA receptor, uPAR, using antibodie and peptides (51, 52). The subsequent translation of uPAR-targeted antibodies failed because of a lack of specificity or humanization affected their affinity. The data presented here document the first time the PAS has been imaged by targeting uPA instead of uPAR using a clinically relevant imaging modality. By targeting uPA instead of uPAR we gain a greater insight into the proteolytic activity of the cancer. Increased proteolysis is a common trait of aggressive cancer with a high metastatic potential and studies have directly correlated increased uPA levels with disease progression and metastasis (22, 53). Because U33 only binds active uPA, U33 directly informs about the amount of uPA activity in the system. The levels of active uPA can change based on the depletion of activating proteases, such as hK2 or MMP-9, due to treatment. This decrease in active uPA could be detected with U33 - decreased proteolytic activity can act as surrogate marker of indolence and regression.

Together our data demonstrate that U33 is a unique, potent and selective active site inhibitor of uPA that can be used to image prostate cancer in preclinical models. While secreted, uPA remains largely restricted to the tumor microenvironment because of its interaction with uPAR. uPA that does escape into circulation is quickly inactivated by macromolecular protease inhibitors. U33 IgG would not bind to complexed uPA in the blood, thus preventing a disseminated imaging probe that would reduce target to non-target ratios. Since both uPA and uPAR are expressed by cancerous prostate cells and tumor-associated stromal cells, our uPA-targeted probe has the ability to detect the tumor cells and the abetting microenvironment with a single agent. Notably, the utility of U33 IgG is not limited to prostate cancer. uPA and the other components of the PAS are over-expressed in a myriad of cancers ranging from ovarian to breast (54). Additionally, U33 IgG has the potential to be both a diagnostic and therapeutic agent. The internalization and clearance from the blood makes U33 IgG an ideal candidate for radioimmunotherapy. The unique mechanism of U33 antibody accumulation in tumors expressing active uPA and uPAR presents significant opportunities for clinical applications from diagnostic imaging to therapeutic intervention.

Supplementary Material

Refer to Web version on PubMed Central for supplementary material.

Acknowledgments

The authors would like to thank Fei Han, Jason Gee, Shouchun Liu and Jeanne Flandez of CytomX Therapeutics Inc. for construction, expression and purification of U33 IgG. This work was supported by the Rogers Family Award (to C.S.C. and H.F.V.) and the National Institutes of Health grant R01 CA128765 (to C.S.C.). A.M.L. was supported by a DOD Prostate Cancer Postdoctoral Award PC094386 and the DOD Idea Award PC111318. A.M.L. is currently the Steve Wynn 2013 Prostate Cancer Foundation Young Investigator.

References

1. Jemal A, Siegel R, Xu J, Ward E. Cancer statistics, 2010. CA Cancer J Clin. 2010; 60:277–300. [PubMed: 20610543]
2. Denmeade SR, Isaacs JT. Development of prostate cancer treatment: the good news. The Prostate. 2004; 58:211–24. [PubMed: 14743459]
3. Schweizer MT, Antonarakis ES. Abiraterone and other novel androgen-directed strategies for the treatment of prostate cancer: a new era of hormonal therapies is born. Ther Adv Urol. 2012; 4:167–78. [PubMed: 22852027]
4. Brassell SA, Rosner IL, McLeod DG. Update on magnetic resonance imaging, ProstaScint, and novel imaging in prostate cancer. Curr Opin Urol. 2005; 15:163–6. [PubMed: 15815192]
5. Keshari KR, Wilson DM. Chemistry and biochemistry of 13C hyperpolarized magnetic resonance using dynamic nuclear polarization. Chemical Society reviews. 2014; 43:1627–59. [PubMed: 24363044]
6. Lawrentschuk N, Davis ID, Bolton DM, Scott AM. Diagnostic and therapeutic use of radioisotopes for bony disease in prostate cancer: current practice. Int J Urol. 2007; 14:89–95. [PubMed: 17302562]
7. Evans MJ. Measuring Oncogenic Signaling Pathways in Cancer with PET: An Emerging Paradigm from Studies in Castration-Resistant Prostate Cancer. Cancer discovery. 2012; 2:985–94. [PubMed: 23043150]
8. Jadvar H. Molecular imaging of prostate cancer with PET. Journal of nuclear medicine : official publication, Society of Nuclear Medicine. 2013; 54:1685–8.
9. Kairemo K, Rasulova N, Partanen K, Joensuu T. Preliminary clinical experience of trans-1-Amino-3-(18)F-fluorocyclobutanecarboxylic Acid (anti-(18)F-FACBC) PET/CT imaging in prostate cancer patients. BioMed research international. 2014; 2014:305182. [PubMed: 24991547]
10. Manyak MJ. Indium-111 capromab pendetide in the management of recurrent prostate cancer. Expert Rev Anticancer Ther. 2008; 8:175–81. [PubMed: 18279057]
11. Rieter WJ, Keane TE, Ahlman MA, Ellis CT, Spicer KM, Gordon LL. Diagnostic performance of In-111 capromab pendetide SPECT/CT in localized and metastatic prostate cancer. Clinical nuclear medicine. 2011; 36:872–8. [PubMed: 21892036]
12. Bander NH, Trabulsi EJ, Kostakoglu L, Yao D, Vallabhajosula S, Smith-Jones P, et al. Targeting metastatic prostate cancer with radiolabeled monoclonal antibody J591 to the extracellular domain of prostate specific membrane antigen. The Journal of urology. 2003; 170:1717–21. [PubMed: 14532761]
13. Cho SY, Gage KL, Mease RC, Senthamizhchelvan S, Holt DP, Jeffrey-Kwanisai A, et al. Biodistribution, tumor detection, and radiation dosimetry of 18F-DCFBC, a low-molecular-weight inhibitor of prostate-specific membrane antigen, in patients with metastatic prostate cancer. Journal of nuclear medicine : official publication, Society of Nuclear Medicine. 2012; 53:1883–91.
14. Li Y, Cozzi PJ. Targeting uPA/uPAR in prostate cancer. Cancer Treat Rev. 2007; 33:521–7. [PubMed: 17658220]

15. Crowley CW, Cohen RL, Lucas BK, Liu G, Shuman MA, Levinson AD. Prevention of metastasis by inhibition of the urokinase receptor. Proceedings of the National Academy of Sciences of the United States of America. 1993; 90:5021–5. [PubMed: 8389464]
16. Rabbani SA, Ateeq B, Arakelian A, Valentino ML, Shaw DE, Dauffenbach LM, et al. An anti-urokinase plasminogen activator receptor antibody (ATN-658) blocks prostate cancer invasion, migration, growth, and experimental skeletal metastasis in vitro and in vivo. Neoplasia. 2010; 12:778–88. [PubMed: 20927316]
17. Logothetis CJ, Lin SH. Osteoblasts in prostate cancer metastasis to bone. Nature reviews Cancer. 2005; 5:21–8.
18. Kirchheimer JC, Pfluger H, Ritschl P, Hienert G, Binder BR. Plasminogen activator activity in bone metastases of prostatic carcinomas as compared to primary tumors. Invasion Metastasis. 1985; 5:344–55. [PubMed: 4066206]
19. Czekay RP, Wilkins-Port CE, Higgins SP, Freytag J, Overstreet JM, Klein RM, et al. PAI-1: An Integrator of Cell Signaling and Migration. Int J Cell Biol. 2011; 2011:562481. [PubMed: 21837240]
20. Mikolajczyk SD, Millar LS, Kumar A, Saedi MS. Prostatic human kallikrein 2 inactivates and complexes with plasminogen activator inhibitor-1. International journal of cancer Journal international du cancer. 1999; 81:438–42. [PubMed: 10209959]
21. Shariat SF, Roehrborn CG, McConnell JD, Park S, Alam N, Wheeler TM, et al. Association of the circulating levels of the urokinase system of plasminogen activation with the presence of prostate cancer and invasion, progression, and metastasis. Journal of clinical oncology : official journal of the American Society of Clinical Oncology. 2007; 25:349–55. [PubMed: 17264329]
22. Shariat SF, Karam JA, Margulis V, Karakiewicz PI. New blood-based biomarkers for the diagnosis, staging and prognosis of prostate cancer. BJU international. 2008; 101:675–83. [PubMed: 17941930]
23. Hienert G, Kirchheimer JC, Pfluger H, Binder BR. Urokinase-type plasminogen activator as a marker for the formation of distant metastases in prostatic carcinomas. The Journal of urology. 1988; 140:1466–9. [PubMed: 3193516]
24. Cozzi PJ, Wang J, Delprado W, Madigan MC, Fairy S, Russell PJ, et al. Evaluation of urokinase plasminogen activator and its receptor in different grades of human prostate cancer. Hum Pathol. 2006; 37:1442–51. [PubMed: 16949925]
25. Kumano M, Miyake H, Muramaki M, Furukawa J, Takenaka A, Fujisawa M. Expression of urokinase-type plasminogen activator system in prostate cancer: correlation with clinicopathological outcomes in patients undergoing radical prostatectomy. Urol Oncol. 2009; 27:180–6. [PubMed: 18439850]
26. Gupta A, Lotan Y, Ashfaq R, Roehrborn CG, Raj GV, Aragaki CC, et al. Predictive value of the differential expression of the urokinase plasminogen activation axis in radical prostatectomy patients. European urology. 2009; 55:1124–33. [PubMed: 18585843]
27. Lebeau AM, Duriseti S, Murphy ST, Pepin F, Hann B, Gray JW, et al. Targeting uPAR with Antagonistic Recombinant Human Antibodies in Aggressive Breast Cancer. Cancer Res. 2013
28. Schmittgen TD, Livak KJ. Analyzing real-time PCR data by the comparative C(T) method. Nature protocols. 2008; 3:1101–8.
29. LeBeau AM, Lee M, Murphy ST, Hann BC, Warren RS, Delos Santos R, et al. Imaging a functional tumorigenic biomarker in the transformed epithelium. Proc Natl Acad Sci U S A. 2013; 110:93–8. [PubMed: 23248318]
30. de Haard HJ, van Neer N, Reurs A, Hufton SE, Roovers RC, Henderikx P, et al. A large non-immunized human Fab fragment phage library that permits rapid isolation and kinetic analysis of high affinity antibodies. The Journal of biological chemistry. 1999; 274:18218–30. [PubMed: 10373423]
31. Sun J, Pons J, Craik CS. Potent and selective inhibition of membrane-type serine protease 1 by human single-chain antibodies. Biochemistry. 2003; 42:892–900. [PubMed: 12549907]
32. Duriseti S, Goetz DH, Hostetter DR, LeBeau AM, Wei Y, Craik CS. Antagonistic anti-urokinase plasminogen activator receptor (uPAR) antibodies significantly inhibit uPAR-mediated cellular

signaling and migration. The Journal of biological chemistry. 2010; 285:26878–88. [PubMed: 20501655]

33. LeBeau AM, Singh P, Isaacs JT, Denmeade SR. Potent and selective peptidyl boronic acid inhibitors of the serine protease prostate-specific antigen. Chemistry & biology. 2008; 15:665–74. [PubMed: 18635003]
34. O'Donoghue AJ, Eroy-Reveles AA, Knudsen GM, Ingram J, Zhou M, Statnekov JB, et al. Global identification of peptidase specificity by multiplex substrate profiling. Nat Methods. 2012; 9:1095–100. [PubMed: 23023596]
35. Park SI, Kim SJ, McCauley LK, Gallick GE. Pre-clinical mouse models of human prostate cancer and their utility in drug discovery. Curr Protoc Pharmacol. 2010; Chapter 14(Unit 14):5.
36. Jo M, Lester RD, Montel V, Eastman B, Takimoto S, Gonias SL. Reversibility of epithelial-mesenchymal transition (EMT) induced in breast cancer cells by activation of urokinase receptor-dependent cell signaling. The Journal of biological chemistry. 2009; 284:22825–33. [PubMed: 19546228]
37. Milosevic M, Warde P, Menard C, Chung P, Toi A, Ishkanian A, et al. Tumor hypoxia predicts biochemical failure following radiotherapy for clinically localized prostate cancer. Clinical cancer research : an official journal of the American Association for Cancer Research. 2012; 18:2108–14. [PubMed: 22465832]
38. Stewart GD, Ross JA, McLaren DB, Parker CC, Habib FK, Riddick AC. The relevance of a hypoxic tumour microenvironment in prostate cancer. BJU Int. 2010; 105:8–13. [PubMed: 19889065]
39. Cheng HH, Mitchell PS, Kroh EM, Dowell AE, Chery L, Siddiqui J, et al. Circulating microRNA Profiling Identifies a Subset of Metastatic Prostate Cancer Patients with Evidence of Cancer-Associated Hypoxia. PLoS One. 2013; 8:e69239. [PubMed: 23935962]
40. Usher PA, Thomsen OF, Iversen P, Johnsen M, Brunner N, Hoyer-Hansen G, et al. Expression of urokinase plasminogen activator, its receptor and type-1 inhibitor in malignant and benign prostate tissue. Int J Cancer. 2005; 113:870–80. [PubMed: 15515049]
41. Shukeir N, Pakneshan P, Chen G, Szyf M, Rabbani SA. Alteration of the methylation status of tumor-promoting genes decreases prostate cancer cell invasiveness and tumorigenesis in vitro and in vivo. Cancer research. 2006; 66:9202–10. [PubMed: 16982764]
42. Pakneshan P, Xing RH, Rabbani SA. Methylation status of uPA promoter as a molecular mechanism regulating prostate cancer invasion and growth in vitro and in vivo. FASEB J. 2003; 17:1081–8. [PubMed: 12773490]
43. Shariat SF, Semjonow A, Lilja H, Savage C, Vickers AJ, Bjartell A. Tumor markers in prostate cancer I: blood-based markers. Acta oncologica. 2011; 50 (Suppl 1):61–75. [PubMed: 21604943]
44. Miyake H, Hara I, Yamanaka K, Gohji K, Arakawa S, Kamidono S. Elevation of serum levels of urokinase-type plasminogen activator and its receptor is associated with disease progression and prognosis in patients with prostate cancer. The Prostate. 1999; 39:123–9. [PubMed: 10221568]
45. Kogianni G, Walker MM, Waxman J, Sturge J. Endo180 expression with cofunctional partners MT1-MMP and uPAR-uPA is correlated with prostate cancer progression. European journal of cancer. 2009; 45:685–93. [PubMed: 19112015]
46. Zhu M, Gokhale VM, Szabo L, Munoz RM, Baek H, Bashyam S, et al. Identification of a novel inhibitor of urokinase-type plasminogen activator. Molecular cancer therapeutics. 2007; 6:1348–56. [PubMed: 17431113]
47. Schweinitz A, Steinmetzer T, Banke IJ, Arlt MJ, Sturzebecher A, Schuster O, et al. Design of novel and selective inhibitors of urokinase-type plasminogen activator with improved pharmacokinetic properties for use as antimetastatic agents. The Journal of biological chemistry. 2004; 279:33613–22. [PubMed: 15150279]
48. Rockway TW, Giranda VL. Inhibitors of the proteolytic activity of urokinase type plasminogen activator. Current pharmaceutical design. 2003; 9:1483–98. [PubMed: 12871064]
49. Sgier D, Zuberbuehler K, Pfaffen S, Neri D. Isolation and characterization of an inhibitory human monoclonal antibody specific to the urokinase-type plasminogen activator, uPA. Protein Eng Des Sel. 2010; 23:261–9. [PubMed: 20086040]

50. Ulmert D, Evans MJ, Holland JP, Rice SL, Wongvipat J, Pettersson K, et al. Imaging androgen receptor signaling with a radiotracer targeting free prostate-specific antigen. Cancer discovery. 2012; 2:320–7. [PubMed: 22576209]

51. Kriegbaum MC, Persson M, Haldager L, Alpizar-Alpizar W, Jacobsen B, Gardsvoll H, et al. Rational targeting of the urokinase receptor (uPAR): development of antagonists and non-invasive imaging probes. Curr Drug Targets. 2011; 12:1711–28. [PubMed: 21707479]

52. Rabbani SA, Gladu J. Urokinase receptor antibody can reduce tumor volume and detect the presence of occult tumor metastases in vivo. Cancer research. 2002; 62:2390–7. [PubMed: 11956102]

53. Gaylis FD, Keer HN, Wilson MJ, Kwaan HC, Sinha AA, Kozlowski JM. Plasminogen activators in human prostate cancer cell lines and tumors: correlation with the aggressive phenotype. The Journal of urology. 1989; 142:193–8. [PubMed: 2659823]

54. Dass K, Ahmad A, Azmi AS, Sarkar SH, Sarkar FH. Evolving role of uPA/uPAR system in human cancers. Cancer Treat Rev. 2008; 34:122–36. [PubMed: 18162327]

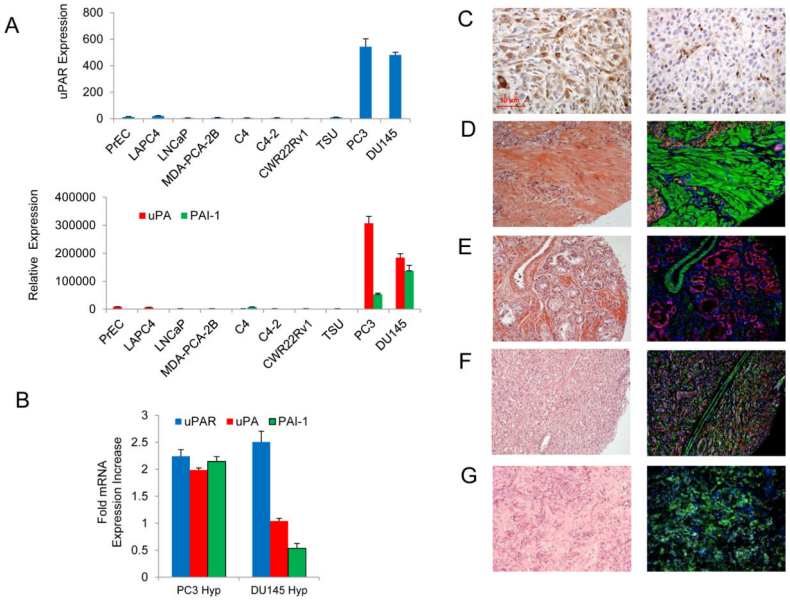

Figure 1.

uPA expression in prostate cancer cell lines and prostate cancer tissue microarray sections. **(A)** mRNA levels of uPAR (top) and uPA and PAI-1 (bottom) were analyzed using quantitative RT-PCR in prostate cancer cell lines and normal human prostate epithelial cells. **(B)** qRT-PCR analysis of the PAS components in PC3 and DU145 cells cultured under 1.5% O_2 for 72hrs. The increase in mRNA expression is compared to the cells grown under normoxia. **(C)** IHC staining of a PC3 xenograft section (left) and a DU145 xenograft section (right) for total uPA protein using the antibody sc-14019. **(D–G)** Visualization of the total uPA protein in prostate cancer tissue microarray sections using immunofluoresence. H&E stained sections are viewed on the left with the merged fluoresence channels on the right with uPA (green), E-caderin (red) and nuclei (DAPI). The sections stained are: **(D)** adenocarcinoma, Gleason score 5 (2 + 3); **(E)** adenocarcinoma, Gleason score 5 (1 + 4); **(F)** adenocarcinoma, Gleason score 9 (4 + 5); **(G)** bone metastasis.

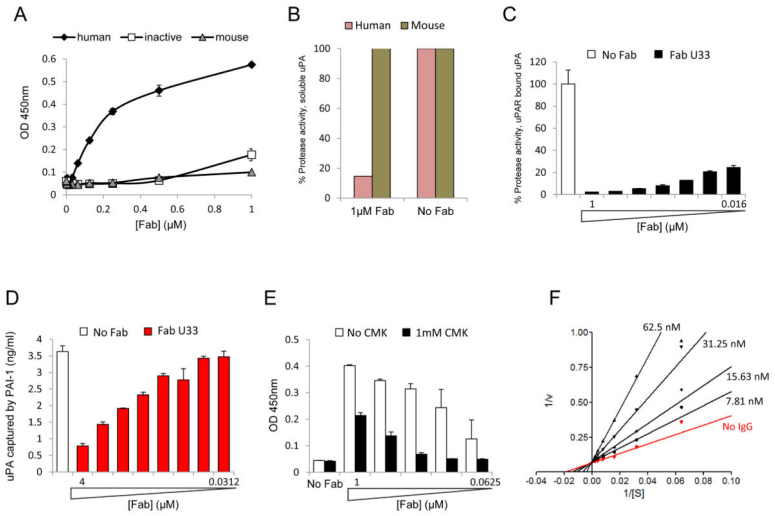

Figure 2.

Characterization of the U33 clone. (**A**) U33 Fab binds specifically to the active form of uPA. Serial dilutions of U33 Fab were added to uPA coated plates and incubated for 1 hour. The amount of Fab bound to uPA was determined by ELISA. U33 Fab was only detected in wells coated with human active uPA. (**B**) Inhibition of human uPA by U33 Fab. The proteolytic activity of human or mouse uPA was read in absence and presence of 1 μM of U33 Fab. The enzyme activity is expressed as percentage of the uPA activity in absence of Fab (100 %). (**C**) Inhibition of uPA bound to uPAR. Serial dilutions of U33 Fab were added to uPAR-uPA coated plates and incubated for 1 hour and the activity of uPA was read. (**D**) U33 Fab prevents uPA binding to PAI-1 coated plates: Serial dilutions of U33 Fab (4 μM to 31.2 nM) were pre-incubated overnight with uPA and added to PAI-1 coated plates. The amount of uPA bound to PAI was determined by ELISA. (**E**) U33 does not bind to uPA inhibited by a CMK inhibitor. Serial dilutions of U33 (0.0625 - 1μM) were added to an uPA coated plate pre-incubated with and without 1 μM CMK. U33 Fab bound to uPA was determined by ELISA. (**F**) Lineweaver-Burke plot demonstrating that U33 IgG is a competitive inhibitor of uPA.

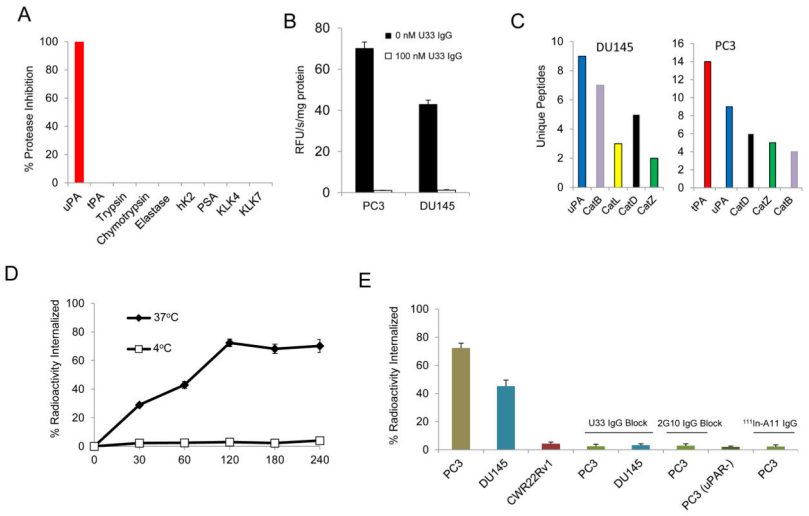

Figure 3.

In vitro characterization studies of U33 IgG. (**A**) Specificity of U33-IgG for uPA compared to a panel of proteases. Proteases were treated with 1μM of U33 IgG in the presence of fluorogenic substrate. (**B**) Inhibition of trypsin-like proteolytic activity in the condition media of PC3 and DU145 cells by U33 IgG. Conditioned media (4.0 μg/ml protein concentration) were incubated with the trypsin cleavable fluorogenic substrate Z-Gly-Gly-Arg-AMC (ex. 355 nm; em. 460 nm) at 400μM in the presence and absence of U33 IgG. **(C**) Mass spectrometry proteomic analysis of secreted proteases from PC3 and DU145 prostate cancer cell lines. The cell lines PC3 and DU145 were cultured for 24hrs under serum-free conditions. The resulting conditioned media were digested with trypsin and the peptides were sequenced on an LTQ-FT ICR mass spectrometer followed by SwissProt database analysis. **(D)** PC3 cellular internalization of ^{111}In-U33 IgG at 37°C and 4°C in conditioned media. PC3 cells were incubated with 10 nM of radiolabeled antibody at the indicated time points and were washed and treated with an acidic buffer to remove non-covalently bound and non-internalized ^{111}In-U33 IgG. Each time point was performed in triplicate. **(E)** Internalization of ^{111}In-U33 IgG at the 120 min time point by the cells lines PC3, DU145, PC3 (uPAR−) and CWR22Rv1 in conditioned media. Blocking was performed by adding 1 μM of cold U33 IgG or 1 μM of 2G10 IgG prior to the media prior to addition of radiolabeled antibody. ^{111}In-A11 IgG was used as the isotype control antibody for the PC3 cells.

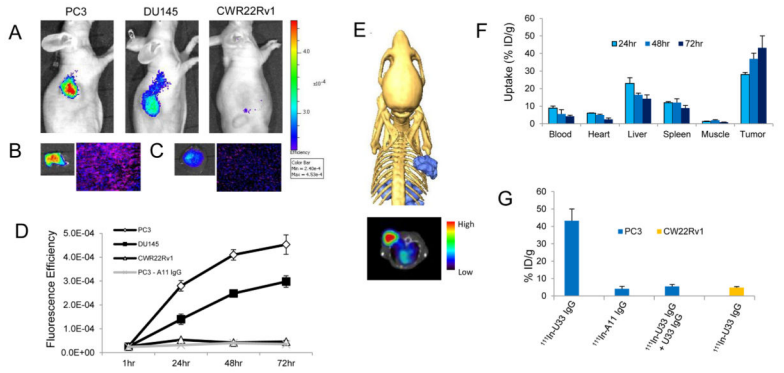

Figure 4.

Molecular imaging and biodistribution of U33 IgG in prostate cancer xenografts. **(A)** Near-infrared (NIR) optical imaging of prostate cancer xenografts using AF680-U33 IgG. Mice bearing PC3, DU145 or CWR22Rv1 xenografts were tail-vein injected with 2 nmol of AF680-U33 IgG and imaged using NIR optical imaging. The images shown are representative of n=3 mice/xenograft and were acquired 72hrs post-injection. (**B**) The resected PC3 tumor at 72hrs fluoresence intensity (*left*) and a tumor section demonstrating probe penetration and localization by fluoresence microscopy (*right*). (**C**) Probe fluoresence intensity (*left*) and localization (*right*) in the liver of a PC3 xenograft mouse. (**D**) Graph depicting the localization of AF680-U33 IgG as fluoresence efficiency of the tumor ROIs for the mice imaged using NIR optical imaging. Included in the graph are the data for the mice imaged with the isotype control AF680-A11 IgG in PC3 xenografts. (**E**) SPECT imaging with ^{111}In-U33 IgG in a PC3 xenograft model. Depicted are SPECT/CT images shown as a three-dimensional volume rendering of the SPECT data (blue) overlaid onto surface rendered CT data and a reconstructed transverse view using a rainbow color scale to show uptake (*below*). Image is representative of n =3 mice imaged with ^{111}In-U33 IgG at 72hrs post-injection. Each animal for imaging received 2.5μg of antibody corresponding to 220 μCi of activity. (**F**) Probe biodistribution was determined by radioactivity assays in PC3 tumor bearing mice (n = 4 for each time point). Tissues were harvested at 24, 48 and 72hrs after injection of ^{111}In-U33 IgG (25 μCi). Probe uptake is reported as percent injected dose per gram (%ID/g). (**G**) Tumor uptake specificity measured at 72hrs post-injection (n = 4 mice for each treatment). PC3 xenograft bearing mice were treated with isotype control ^{111}In-A11 IgG (25μCi) and ^{111}In-U33 IgG blocked (80% reduction) by i.v. pre-injection of 200 μg of cold U33 IgG. Probe uptake in CWR22Rv1 xenografts is also depicted.

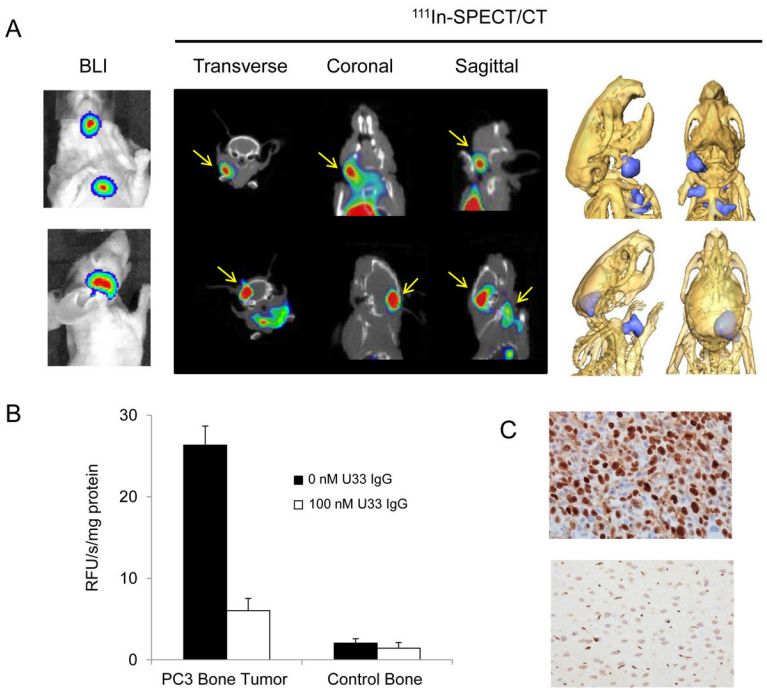

Figure 5.

Imaging active uPA in the PC3 cardiac dissemination model with ^{111}In-U33 IgG. (**A**) 2D and 3D reconstructed ^{111}In-SPECT/CT images of ^{111}In-U33 IgG showing co-localization of the metastatic lesions with the bioluminesence imaging (BLI) data. Yellow arrows denote tumor location in the 2D images (top) Images showing the localization of the anti-uPA probe to an osseous metastatic lesion in the left mandible of the mouse (top) and probe localization to an infiltrating skull lesion and lymph node lesions (bottom). (**B**) Inhibition of the trypsin-like proteolytic activity by U33 IgG in the supernatant from the homogenized mandible lesion and control tissue. Supernatant from both homogenates (2.5μg/ml protein concentration) were assayed for proteolytic activity using Z-Gly-Gly-Arg-AMC (400 μM) in the presence and absence of 100 nM U33 IgG. (**c**) The imaged brain lesion was fixed, sectioned and stained for Ki-67. Intense staining for Ki-67 is apparent in the cancerous lesion (top) compared to normal adjacent brain tissue (bottom).